

## Measurement of the Spin-Forbidden Dark Excitons in MoS<sub>2</sub> and MoSe<sub>2</sub> monolayers

C. Robert<sup>1\*†</sup>, B. Han<sup>1\*†</sup>, P. Kapuscinski<sup>2,3†</sup>, A. Delhomme<sup>2</sup>, C. Faugeras<sup>2\*</sup>, T. Amand<sup>1</sup>, M.R. Molas<sup>4</sup>, M. Bartos<sup>2,5</sup>, K. Watanabe<sup>6</sup>, T. Taniguchi<sup>6</sup>, B. Urbaszek<sup>1</sup>, M. Potemski<sup>2,4</sup> & X. Marie<sup>1</sup>

<sup>1</sup>University of Toulouse, INSA-CNRS-UPS, LPCNO, 135 Av. Rangueil, 31077 Toulouse, France

<sup>2</sup>Laboratoire National des Champs Magnétiques Intenses, CNRS-UGA-UPS-INSA-EMFL, 38042 Grenoble, France

Institute of Experimental Physics, Faculty of Physics, University of Warsaw, ul. Pasteura 5, 02-093 Warsaw, Poland

<sup>3</sup>Wrocław University of Science and Technology, 50-370 Wrocław, Poland

<sup>4</sup>Institute of Experimental Physics, Faculty of Physics, University of Warsaw, 02-093 Warsaw, Poland

<sup>5</sup>Central European Institute of Technology, Brno University of Technology, Purkynova 656/123, 61200 Brno, Czech Republic

<sup>6</sup>National Institute for Materials Science, Tsukuba, Ibaraki 305-0044, Japan

*Excitons with binding energies of a few hundreds of meV control the optical properties of transition metal dichalcogenide monolayers. Knowledge of the fine structure of these excitons is therefore essential to understand the optoelectronic properties of these 2D materials. Here we measure the exciton fine structure of MoS<sub>2</sub> and MoSe<sub>2</sub> monolayers encapsulated in boron nitride by magneto-photoluminescence spectroscopy in magnetic fields up to 30 T. The experiments performed in transverse magnetic field reveal a brightening of the spin-forbidden dark excitons in MoS<sub>2</sub> monolayer: we find that the dark excitons appear at 14 meV below the bright ones. Measurements performed in tilted magnetic field provide a conceivable description of the neutral exciton fine structure. The experimental results are in agreement with a model taking into account the effect of the exchange interaction on both the bright and dark exciton states as well as the interaction with the magnetic field.*

**Introduction.** - Transition Metal Dichalcogenide (TMD) monolayers such as MoS<sub>2</sub>, MoSe<sub>2</sub>, WS<sub>2</sub> or WSe<sub>2</sub> are 2D semiconductors characterized by very strong interaction with light due to robust excitons with large oscillator strengths<sup>1,2,3,4,5</sup>. As for all semiconductor nanostructures the exciton fine structure dictates the efficiency of the coupling to light. One can expect that the optoelectronic properties will change drastically whether the spin-forbidden dark excitons lie below or above the bright excitons<sup>6,7,8,9</sup>. Exciton spin relaxation is also expected to be affected by the bright-dark exciton ordering<sup>10,11</sup>. The main difficulty to experimentally determine the energy of spin-forbidden dark excitons is their extremely small oscillator strength compared to the bright exciton one. The exciton fine structure splitting was accurately determined for WS<sub>2</sub> and WSe<sub>2</sub> monolayers (ML) using various experimental techniques<sup>12,13,14,15</sup>. These measurements were successful only in WSe<sub>2</sub> and WS<sub>2</sub> materials as the dark exciton lie several tens of meV below the bright one so that the small oscillator strength is compensated by a very large population of dark excitons making them observable in photoluminescence experiments. In contrast the respective alignment of bright and dark excitons in MoS<sub>2</sub> ML remains controversial though this material is the most studied among the 2D semiconductors and this was the first member of the TMD family to be established as a direct gap in the monolayer form.

Numerous ab-initio calculations have been proposed to predict the exciton bright-dark splitting but the results are highly dispersed with values in the range 10-40 meV and more importantly with different signs: depending on the methods applied, dark excitons lie above or below the dark ones<sup>16,17,18,19</sup>. It is therefore crucial to have a clear experimental determination.

Unfortunately, all attempts to measure the bright-dark splitting in MoS<sub>2</sub> ML were not conclusive so far. The main reasons given were related to (i) the low optical quality of samples (without hBN encapsulation)<sup>13</sup>, (ii) the small value of the expected splitting compared to the luminescence/absorption linewidth or (iii) the low thermal population of the dark states if they lie above the bright ones<sup>12</sup>.

In this letter, we present the first unambiguous optical emission spectrum of the dark exciton in MoS<sub>2</sub> ML. In contrast to most predictions our measurements demonstrate that the spin-forbidden dark exciton lies below the bright exciton with a bright-dark splitting of +14 meV.

To this end, we performed magneto-photoluminescence experiments up to 30 T on MoS<sub>2</sub> monolayers encapsulated in hexagonal Boron Nitride (hBN) with a magnetic field oriented along the monolayer plane (Voigt geometry). The high quality of the investigated samples allowed us to determine accurately the bright-dark energy splitting. We performed similar measurements in MoSe<sub>2</sub> MLs encapsulated in hBN where a bright-dark splitting of -1.3 meV is determined in agreement with a recent report<sup>20</sup>. Measurements performed in a tilted magnetic field (45° with respect to the ML plane) confirm the spin-forbidden nature of the observed transitions and allow us to provide a conceivable description of the neutral exciton fine structure. The in-plane field component yields a brightening of the dark states and the out-of plane component induces a Zeeman splitting of these states yielding the first measurements of the dark exciton g factor in MoS<sub>2</sub> and MoSe<sub>2</sub> monolayers. Remarkably we find that the energy splitting between the bright and dark excitons in MoSe<sub>2</sub> ML is very similar to the short range exchange energy which splits the two dark exciton states, a very original and unique situation for semiconductor nanostructures.

**Mixing of exciton states in magnetic field.** - First, let us recall that the point symmetry group of a TMD monolayer is D<sub>3h</sub>. The direct band gap is located at the edges of hexagonal Brillouin zone, at the non-equivalent valleys K<sub>±</sub>. Because of the large spin-orbit splitting in the valence band, we restrict here our description to A excitons composed of an electron from one of the two conduction bands split by the spin-orbit interaction Δ<sub>SO</sub> and a hole from the upper valence band A. We also consider only direct excitons (with a center of mass wave-vector K=0). Then the exciton fine structure includes the two optically active (bright) excitons X<sub>B</sub> with parallel spin ↑↑, ↓↓ (symmetry Γ<sub>6</sub>) and the two spin-forbidden dark states X<sub>G</sub>(↑↓ + ↓↑) and X<sub>D</sub>(↑↓ - ↓↑) (symmetry Γ<sub>4</sub> and Γ<sub>3</sub> respectively). The inset of Fig. 1c shows the bright-dark splitting Δ and the grey-dark splitting due to exciton exchange energy. It was shown that these dark states are optically forbidden for in-plane polarized light but that the X<sub>G</sub> (Γ<sub>4</sub>) state can couple to out-of plane polarized light (Oz direction)<sup>12,21,22</sup> and because of this is called here “grey” exciton.

An in-plane magnetic field B<sub>//</sub> (Voigt geometry) mixes the spin components of the 2D exciton states<sup>23,24</sup>. For a TMD monolayer, this field interacts with the conduction band electron within the exciton and we can neglect its interaction with the hole because of the very large valence band spin-orbit splitting<sup>13,14</sup>. As a consequence the in-plane magnetic field brightens both X<sub>G</sub> and X<sub>D</sub> dark exciton states; the mixed bright-dark exciton states couple to in-plane polarized light allowing a straightforward determination of the energy of the dark states<sup>13,14</sup>. On the other hand, an out-of plane magnetic field B<sub>z</sub> (Faraday geometry) leads to the Zeeman splitting of both bright and dark states and to the mixing between X<sub>G</sub> and X<sub>D</sub><sup>21</sup>. Thus, in tilted magnetic field, the four excitons are mixed and split so that it becomes possible to extract the g-factor of dark excitons. The (4x4) Hamiltonian describing the mixing between the four states under a given field with an angle θ with respect to the normal of the ML plane (θ=90° for Voigt and θ=0° for Faraday geometries) is described in the SI6.

**Magneto-photoluminescence for in-plane magnetic field.** - First we have investigated the effect of an in-plane magnetic field (Voigt configuration) on the low temperature photoluminescence spectra in MoS<sub>2</sub> monolayer. The 2D color map of PL intensity as a function of magnetic field from 0 T to 30 T is plotted in Fig. 1a. In zero field, the emission is composed of a unique line corresponding to the radiative recombination of the bright exciton X<sub>B</sub> at 1.931 eV in agreement with previous reports<sup>25</sup>.

Remarkably we observe at low energy, typically 14 meV below  $X_B$ , an additional peak which shows up above  $\sim 12$  T. This feature, interpreted as the brightened spin-forbidden dark exciton, has been reproduced on several samples and spot positions (see data in SI2). In principle, this line should correspond to both brightened grey and dark excitons, but the inhomogeneous linewidth in our samples is too broad to enable us to distinguish the expected small splitting  $\delta$  between grey and dark states. In a simple two-level system where the in-plane magnetic field couples the bright and dark states, one expects that the ratio between the PL intensity of the bright and the dark PL lines follows a simple quadratic law :  $I_D / I_B \sim (B_{//})^2$ , where  $B_{//}$  is the in-plane magnetic field<sup>14</sup>. In Fig. 1c we present the magnetic field dependence of the ratio between the PL intensity of the low energy and the high energy lines (corresponding to exciton states dominated by dark and bright components respectively). The measured quadratic behavior is a strong indication that the low energy line corresponds to the recombination of the dark excitons which have been brightened by the application of the magnetic field. An additional evidence for assigning the low-energy line observed for large in-plane magnetic field to spin forbidden dark excitons is the measurements of its g factor in an external field perpendicular to the monolayer. The measurements in the tilted field geometry presented below yield  $g_z^D = -6.5$ ; this large value is in good agreement with the predicted one in a simple model<sup>26</sup> and the measured one in WSe<sub>2</sub> MLs<sup>21,27</sup> (see table I). To the best of our knowledge this is the first direct experimental evidence of the spin-forbidden dark exciton in MoS<sub>2</sub> monolayer.

We have also evidenced the energy of the spin-forbidden dark exciton in MoSe<sub>2</sub> MLs encapsulated in hBN using the same experimental approach. As shown in the 2D color map of the PL spectra in Voigt configuration presented in Fig. 2a, the brightened dark exciton line (labelled for simplicity  $X_D$ ) lies above the bright exciton one ( $X_B$ ) in contrast to MoS<sub>2</sub> (compare with Fig. 1a). Moreover, the brightened dark exciton starts to be visible at much lower field ( $\sim 8$  T) and the energy of the two lines vary much strongly with  $B_{//}$  as a consequence of the much smaller bright-dark splitting  $\Delta$ . Again, the linewidth of the transitions does not allow us to observe the splitting between grey and dark excitons. Using the general Hamiltonian presented in the SI6., including the effect of the exciton exchange interaction and the external magnetic field (with arbitrary orientation  $\theta$  with respect to the ML plane), we can easily calculate the  $B_{//}$  field dependence of the bright, grey and dark exciton energies. Taking  $\theta = 90^\circ$  (Voigt geometry) and  $\delta = 0.6$  meV, we can fit our data (black solid lines in fig.2b) with  $\Delta = -1.4 \pm 0.1$  meV and  $g_{//} = 2.0 \pm 0.2$ . These values are in good agreement with very similar measurements published very recently<sup>20</sup>. Note that the fit is very weakly sensitive to the value of  $\delta$  for  $\delta < 1$  meV.

In MoTe<sub>2</sub> ML encapsulated with hBN, our measurements did not reveal any new PL line at high magnetic field that could have been attributed to spin-forbidden dark excitons. Our interpretation is that these excitons have a higher energy compared to the bright ones. Thus a very small thermal population of dark states is expected and a much larger magnetic field is required to mix them with bright excitons. This is consistent with the fact that the calculated CB spin-orbit splitting is twice as large as for MoTe<sub>2</sub> as for MoSe<sub>2</sub><sup>19</sup>.

### Magneto-photoluminescence in tilted magnetic field

In order to have a full description of the exciton fine structure, we have measured the PL spectra of MoS<sub>2</sub> and MoSe<sub>2</sub> monolayers in a tilted magnetic field configuration (the field is oriented  $45^\circ$  with respect to the 2D layer plane). These experiments allow the determination of several key parameters, such as the dark exciton g factors. In an oversimplified description, one can consider separately the effect of the two field components on the exciton spectra. The in-plane component of the field yields the mixing of the bright and dark exciton as already observed in the Voigt configuration and the out-of plane component leads to a Zeeman splitting of the states. While the energy splitting between the two spin/valley states for the bright exciton depends linearly with this z-component field (the slope given by effective g factor), the field dependence of the dark states is more complicated since the two

dark states at zero field are split by the exchange energy  $\delta$  of the order of a few hundreds of  $\mu\text{eV}$ <sup>21,27</sup> (inset of Fig. 1c).

First we present the dependence of the PL spectra of MoSe<sub>2</sub> monolayer in tilted magnetic field. At high magnetic field (above  $\sim 12$  T), the color map of the PL intensity in Fig. 3a and the PL spectra in Fig. 3b clearly evidence 4 lines corresponding to the 4 exciton states whose energy vary almost linearly with the field in the range 15-30 T (*i.e.* the out-of plane component varying from  $\sim 10$  to 21 T). For lower magnetic field values, the energy splitting between the states is comparable to the PL linewidth preventing an accurate determination of the energy of the 4 states. However, we observe a clear non-linear dependence of the energy of the main PL line (which corresponds at B=0 to the bright exciton) (see Fig. 3c). This is a consequence of both the effect of the zero-field bright-dark splitting  $\Delta$  and the zero-field splitting between the grey and dark states  $\delta$ .

Thus the rigorous description requires to consider both the exciton interaction with the tilted magnetic field  $\mathbf{B}=\mathbf{B}_{//}+\mathbf{B}_z$  and the exciton exchange interaction;  $B_{//}=B\sin\theta$  and  $B_z=B\cos\theta$  are the magnetic field components parallel and perpendicular to the monolayer plane (in the experiments of Fig. 3,  $\theta=45^\circ$ ). The interaction with the magnetic field is driven by  $g_z^B$  and  $g_z^D$ , which are respectively the exciton g factor of bright and dark excitons and  $g_{//}$ , which is the in-plane electron g factor. The eigenstates for each magnetic field value have been obtained numerically (see SI6). On the basis of this model and using the values  $\Delta=-1.4$  meV and  $g_{//}=2$  obtained from the Voigt experiments (Fig. 2), one can fit simultaneously the field dependence of the energy of the 4 lines presented in Fig. 3c (see the solid line for the calculated curves). The agreement between the experiment and theory is very good. Interestingly, a clear anti-crossing is evidenced in the low field region as a consequence of the interplay of the transverse and longitudinal field components. This fitting procedure yields the g-factor of both the bright and dark states: we find  $g_z^B=-4.0$  and  $g_z^D=-8.63$ . The value of the dark exciton g factor around -9 is very similar to WSe<sub>2</sub> ML<sup>21,27</sup>; it is an additional proof of the highlighting of the spin-forbidden dark states. As we cannot extract the energy of the 4 lines at weak magnetic field due their linewidths, the fit is not very sensitive to the zero field splitting  $\delta$  between the grey and dark states (the curves have been calculated for  $\delta=0.6$  meV, the value measured in WSe<sub>2</sub> ML<sup>21,27</sup>). Note that the labeling of the 4 lines ( $X_B, X_B, X_D, X_G$ ) in Fig.3 is only valid at zero field and for the sake of simplicity we maintain this labelling at high field though the 4 states are strongly mixed. (See SI7 for the calculation of the weight of the 4 components at high field).

Finally we have measured the excitons spectra of MoS<sub>2</sub> ML in tilted magnetic field. Due to the larger PL linewidth compared to the one of MoSe<sub>2</sub> ML, it is more difficult to evidence the 4 excitons states as in Fig. 3a. However the energy of the two Zeeman split dark states can be extracted above 15 T as shown in Fig. 4(a). Fig. 4(b) displays the measured magnetic field dependence of the energies of the four states together with the fit based on the same model as MoSe<sub>2</sub>. (The raw data as a color plot is shown in SI5). Using  $\Delta=+14.0$  meV and  $g_{//}=2$  (determined previously in the Voigt geometry), the best fit is obtained for  $g_z^B=-1.8$  and  $g_z^D=-6.5$ . The bright exciton g-factor of about -2 was already measured in high quality MoS<sub>2</sub> monolayer<sup>28</sup>. However this is here the first measurement of the dark exciton g factor. Interestingly, we note that the g factors of both bright and dark excitons are significantly smaller in MoS<sub>2</sub> than in other TMD materials. We can speculate that this is due to the very small conduction band spin-orbit splitting. Similarly, to MoSe<sub>2</sub>, the fit is not sensitive to the value of the dark-grey splitting due to the lack of experimental data at low field (the calculation has been done for  $\delta=0.6$  meV). Table I summarizes the parameters of the exciton fine structure of MoS<sub>2</sub> and MoSe<sub>2</sub> monolayers presented in this Letter, together with the ones of WS<sub>2</sub> and WSe<sub>2</sub> MLs from previous work.

## Discussion

The measured value of  $\Delta=14$  meV in MoS<sub>2</sub> ML generates several remarks and interrogations.

(i) First it demonstrates the key role played by the exciton exchange energy contribution to the bright-dark energy splitting. The bright-dark exciton splitting  $\Delta$  includes three contributions<sup>18,19,17</sup>:

$\Delta = \Delta_{SO} + \Delta_{bind} + \Delta_{exch.}$ , where  $\Delta_{SO}$  is the conduction band spin-orbit splitting,  $\Delta_{bind}$  is the difference between the binding energies of bright and dark excitons due to the slightly different masses of spin  $\uparrow$

and spin  $\downarrow$  conduction bands and  $\Delta_{\text{exch}}$  is the short range exciton exchange energy. Although the actual value of the spin-orbit splitting is not yet known, the most widely used calculated value in the literature is  $\Delta_{\text{SO}} = -3$  meV<sup>29</sup>. The calculated binding energy difference on the basis of the calculated mass<sup>29</sup> and the exciton binding energy<sup>30</sup> is  $\Delta_{\text{bind}} = +8$  meV. As a consequence our measurement of  $\Delta = +14$  meV demonstrates that the exciton exchange energy is crucial to determine the amplitude and the sign of the bright-dark energy splitting. Thus we deduce  $\Delta_{\text{exch}} \sim +9$  meV (if indeed  $\Delta_{\text{SO}} = -3$  meV and  $\Delta_{\text{bind}} = +8$  meV). Note that the CB spin-orbit splitting in MoS<sub>2</sub> monolayer has been recently estimated from transport measurements<sup>31</sup>; a splitting of about 15 meV was measured for an electron density of a few  $10^{12}$  cm<sup>-2</sup>. This value 5 times larger than the calculated one includes significant band renormalization induced by many body effects.

(ii) Importantly our measurements show that the splitting between spin-forbidden bright and dark excitons in MoS<sub>2</sub> ML has an opposite sign compared to the calculated spin-orbit splitting in the conduction band. This could have important consequences for the trion fine structure<sup>32</sup>.

(iii) Our measurements raise the question of the simple interpretation of MoS<sub>2</sub> as a “bright” material. Indeed the TMD monolayers are usually divided into two categories: the so-called “dark” materials such as WS<sub>2</sub> and WSe<sub>2</sub> MLs where the spin-forbidden dark excitons lie at lower energy compared to the bright ones. As a consequence these monolayers are characterized by a rather weak luminescence yield at low temperature while the intensity increases with temperature due to thermal activation of bright states<sup>6,7,8,9</sup>. In contrast MoX<sub>2</sub> monolayer (X=S, Se or Te) are often considered as “bright” materials as they exhibit stronger PL intensity at low temperature than their W-based counterparts but their intensity drops with temperature. This difference was assumed to vouch for dark excitons lying above the bright ones in MoX<sub>2</sub>. This bright-dark ordering has indeed been observed very recently for MoSe<sub>2</sub> ML<sup>20</sup> and confirmed by our results presented above. The measurements displayed in Fig. 1 show that the ordering is surprisingly opposite in MoS<sub>2</sub> ML although the temperature dependence of the PL intensity in MoS<sub>2</sub> ML is very similar to MoSe<sub>2</sub> (strong at low temperature and decrease when temperature increases). In addition, one can wonder why the grey exciton cannot be detected at zero magnetic field using high numerical aperture objective like in WS<sub>2</sub> and WSe<sub>2</sub><sup>12</sup>. Remarkably we note in Fig. 1 that the PL intensity of the mixed dark-bright state in transverse magnetic field is very weak (compared to similar experiments performed in WS<sub>2</sub> or WSe<sub>2</sub> MLs<sup>12,13</sup>) and that very high field are required to sizably observe it (larger than 14 T). We can speculate that either the oscillator strength of grey exciton is much smaller than in WX<sub>2</sub> and/or that their population remains weak despite lying at lower energy than the bright state. We can tentatively explain the small oscillator strength by noticing that the smaller spin-orbit interaction in MoS<sub>2</sub> compared to WS<sub>2</sub> or WSe<sub>2</sub> may yield a weaker oscillator strength of the grey exciton since it is related to the spin-orbit mixing with higher energy bands<sup>12,19</sup>. For the population issue, we can notice that contrary to WX<sub>2</sub>, the bright-dark exciton splitting in MoS<sub>2</sub> ML is smaller than the optical phonon energies<sup>3,33</sup> which can lead to inefficient relaxation between bright and dark excitons.

Our results also raise some questions about the interpretation of the very large emission efficiency (almost unity) claimed in acid-treated MoS<sub>2</sub> at room temperature<sup>34</sup>. Assuming a thermodynamic equilibrium between bright and dark states and  $\Delta = +14$  meV, the lower energy spin-forbidden dark excitons states should trap almost half of the population at room temperature, yielding a reduced photoluminescence intensity. Further investigations beyond the topic of this work will be required to answer this question.

Another striking difference between TMD materials is the amplitude of spin/valley polarization for excitons. While strong valley polarization and valley coherence have been measured in WSe<sub>2</sub>, WS<sub>2</sub> and MoS<sub>2</sub> MLs, the polarization in MoSe<sub>2</sub> and MoTe<sub>2</sub> MLs is very weak<sup>35,36</sup>. Recently, it was proposed that a crossing of bright and dark exciton dispersion curves combined with a Rashba effect associated with local fluctuations of electric field can lead to very fast spin relaxation<sup>11</sup>. Our measurements of bright dark splitting in MoS<sub>2</sub> and MoSe<sub>2</sub> are perfectly consistent with this scenario: the small negative splitting  $\Delta = -1.4$  meV in MoSe<sub>2</sub> combined with a larger effective mass for dark excitons should lead to a crossing between bright and dark dispersions while the positive splitting  $\Delta = +14$  meV in MoS<sub>2</sub> guarantees no

crossing and as a consequence significant spin/valley exciton polarization measured in MoS<sub>2</sub> MLs under cw optical orientation experiments <sup>37,38,39</sup>.

In conclusion we have performed magneto-photoluminescence experiments in transverse and tilted magnetic fields up to 30 T in high quality MoS<sub>2</sub> and MoSe<sub>2</sub> monolayers. These investigations yield the unambiguous determination of the bright-dark exciton splitting and the dark exciton g-factor. Such fundamental parameters are key elements to understand the optoelectronic and spin/valley properties of these 2D semiconductors as well as their associated van der Waals heterostructures.

### Methods.

High-quality MoS<sub>2</sub> and MoSe<sub>2</sub> MLs encapsulated in hexagonal boron nitride (hBN) and transferred onto an SiO<sub>2</sub> (80 nm)/Si substrate have been fabricated. Details on sample fabrication can be found in the Supplementary Information (SI) and in Refs<sup>12,40</sup>.

Magneto-PL experiments at 4.2 K are performed in the Voigt configuration (magnetic field parallel to the layer plane) or tilted configuration (field oriented 45° with respect to the ML plane) using an optical-fiber-based insert placed in a high static magnetic field resistive magnet producing fields up to 30 T (see SI1).

### Acknowledgements.

We acknowledge funding from ANR 2D-vdW-Spin, ANR VallEx, ANR MagicValley, ANR Graskop (ANR-19-CE09-0026) projects, Labex NEXT projects VWspin and MILO, EU Graphene Flagship project (no.785219), ATOMOPTO project (TEAM programme of the Foundation for Polish Science, co-financed by the EU within the ERD Fund), National Science Centre, Poland (grant no.UMO-2018/31/B/ST3/02111), and ME-YS-Czech Republic CEITEC 2020 (LQ1601) project. K.W. and T.T. acknowledge support from the Elemental Strategy Initiative conducted by the MEXT, Japan and and the CREST (JPMJCR15F3), JST. X. M. also acknowledges the Institut Universitaire de France.

\* CR, BH and PK contributed equally to this work.

† Corresponding Authors : [cerobert@insa-toulouse.fr](mailto:cerobert@insa-toulouse.fr), [bhan@insa-toulouse.fr](mailto:bhan@insa-toulouse.fr), [clement.faugeras@lncmi.cnrs.fr](mailto:clement.faugeras@lncmi.cnrs.fr),

	MoS <sub>2</sub>	MoSe <sub>2</sub>	WSe <sub>2</sub>	WS <sub>2</sub>
Splitting between bright and dark exciton $\Delta$ (meV)	+14	-1.4	+40 <sup>12,15</sup>	+55 <sup>12</sup>
Splitting between grey and dark excitons $\delta$ (meV)	< 2	< 1	0.6 <sup>21,27</sup>	-
Bright exciton g factor	-1.8	-4.0	-4.25 <sup>41</sup>	-4.0 <sup>30</sup>
Dark exciton g factor	-6.5	-8.6	-9.4 <sup>21,27</sup>	-
Transverse electron g factor	2	2	2	-

Table I : Measured exciton fine structure parameters for hBN encapsulated TMD monolayers

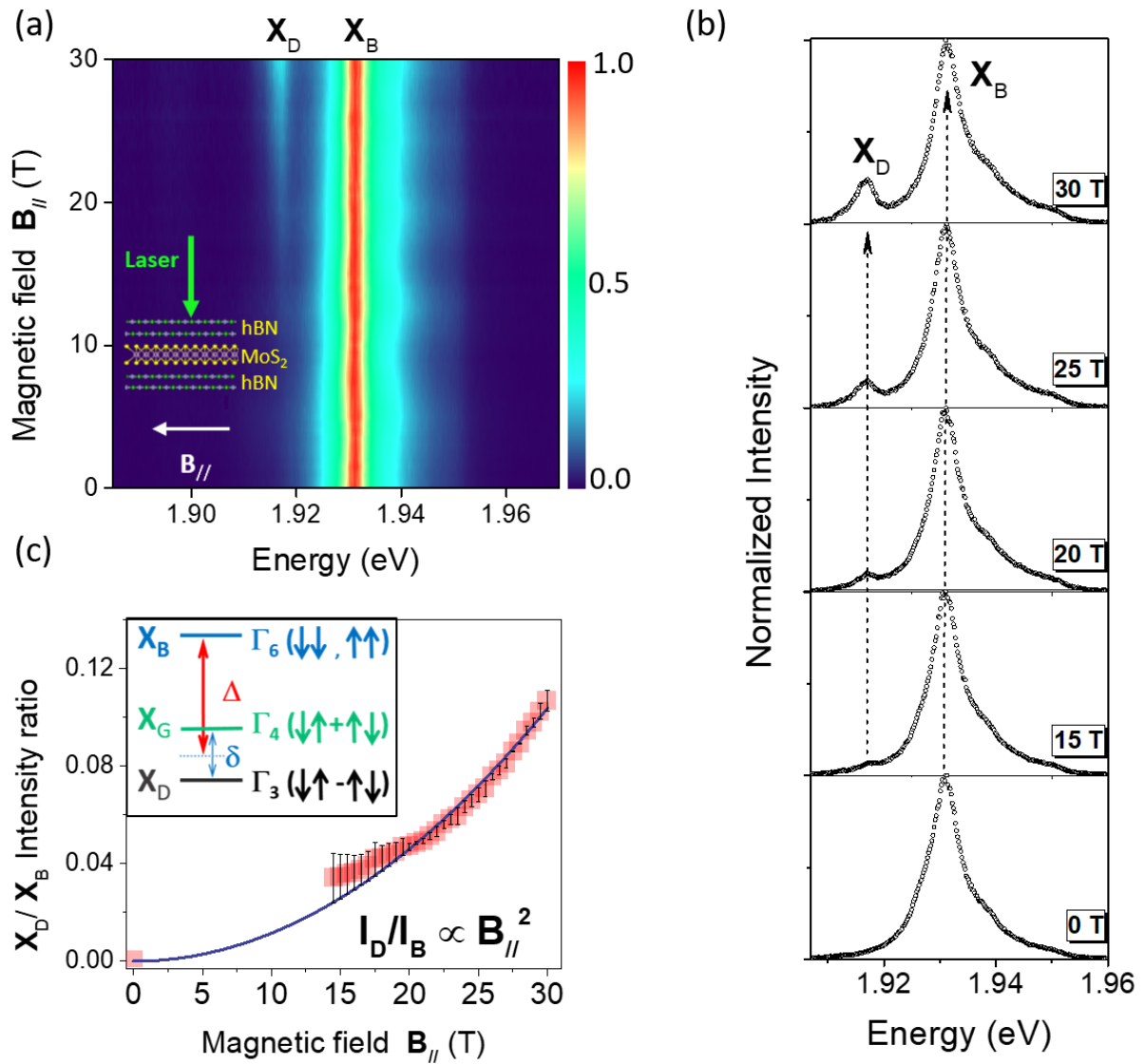


Figure 1 -In-plane magnetic field  $B_{//}$  – Spin-forbidden dark exciton in MoS<sub>2</sub> monolayer encapsulated in hBN revealed by photoluminescence. (a) Color map of the variation of the PL intensity as a function of  $B_{//}$  (the PL intensity of the bright exciton has been normalized at each field); (b) PL spectra for magnetic fields from 0 to 30 T showing the emergence of the brightened dark exciton at low energy. (c) Ratio of the PL intensity of dark ( $X_D$ ) and bright ( $X_B$ ) excitons as a function of magnetic field. Inset: sketch of the excitonic fine structure.

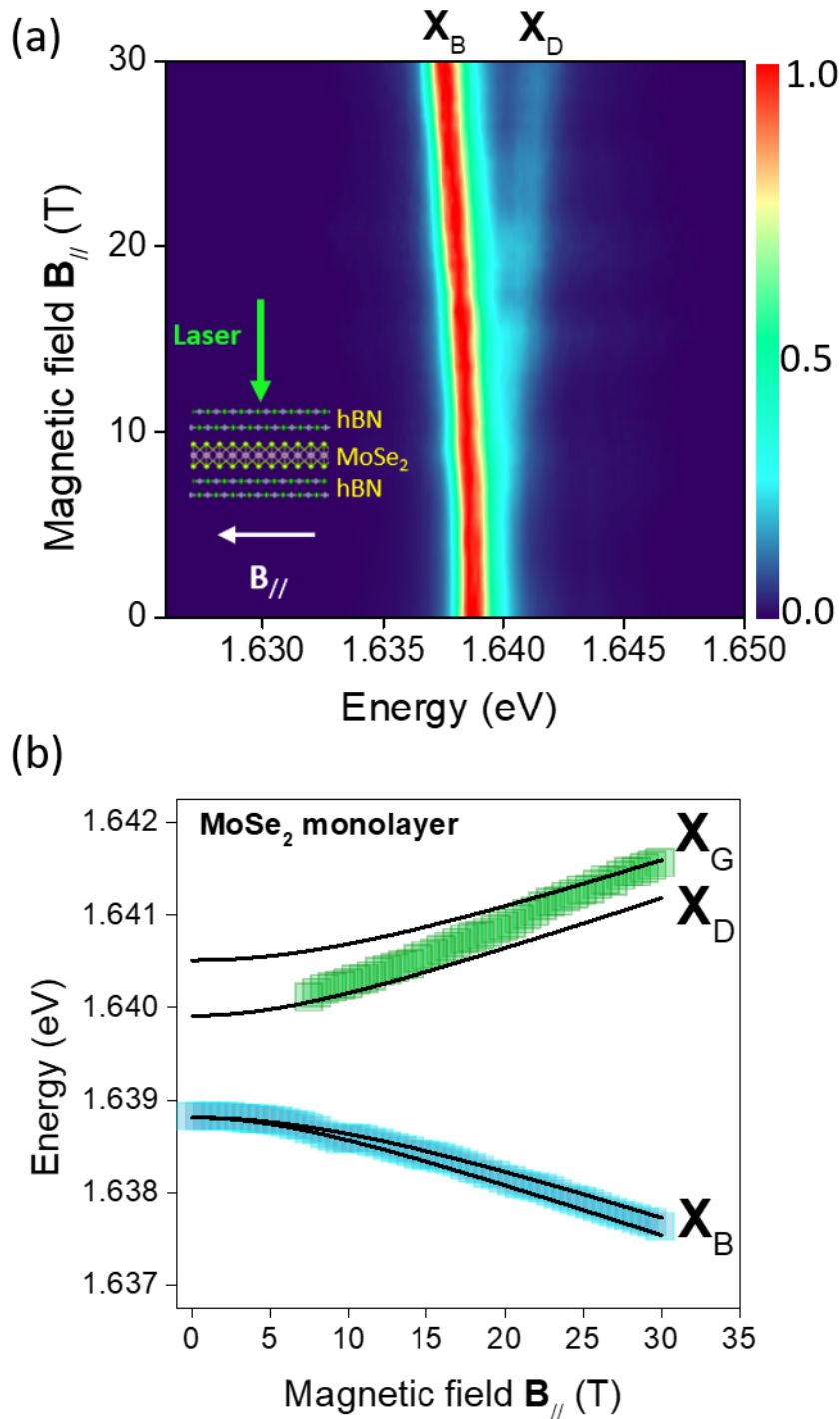


Figure 2 -In-plane magnetic field  $B_{//}$  – Spin-forbidden dark exciton in MoSe<sub>2</sub> monolayer encapsulated in hBN revealed by photoluminescence. (a) Color map of the variation of the PL intensity as a function of  $B_{//}$  (the PL intensity of the bright exciton has been normalized at each field); (b) Energy of dark and bright excitons as a function of  $B_{//}$ . The solid lines correspond to the fit described in the text.



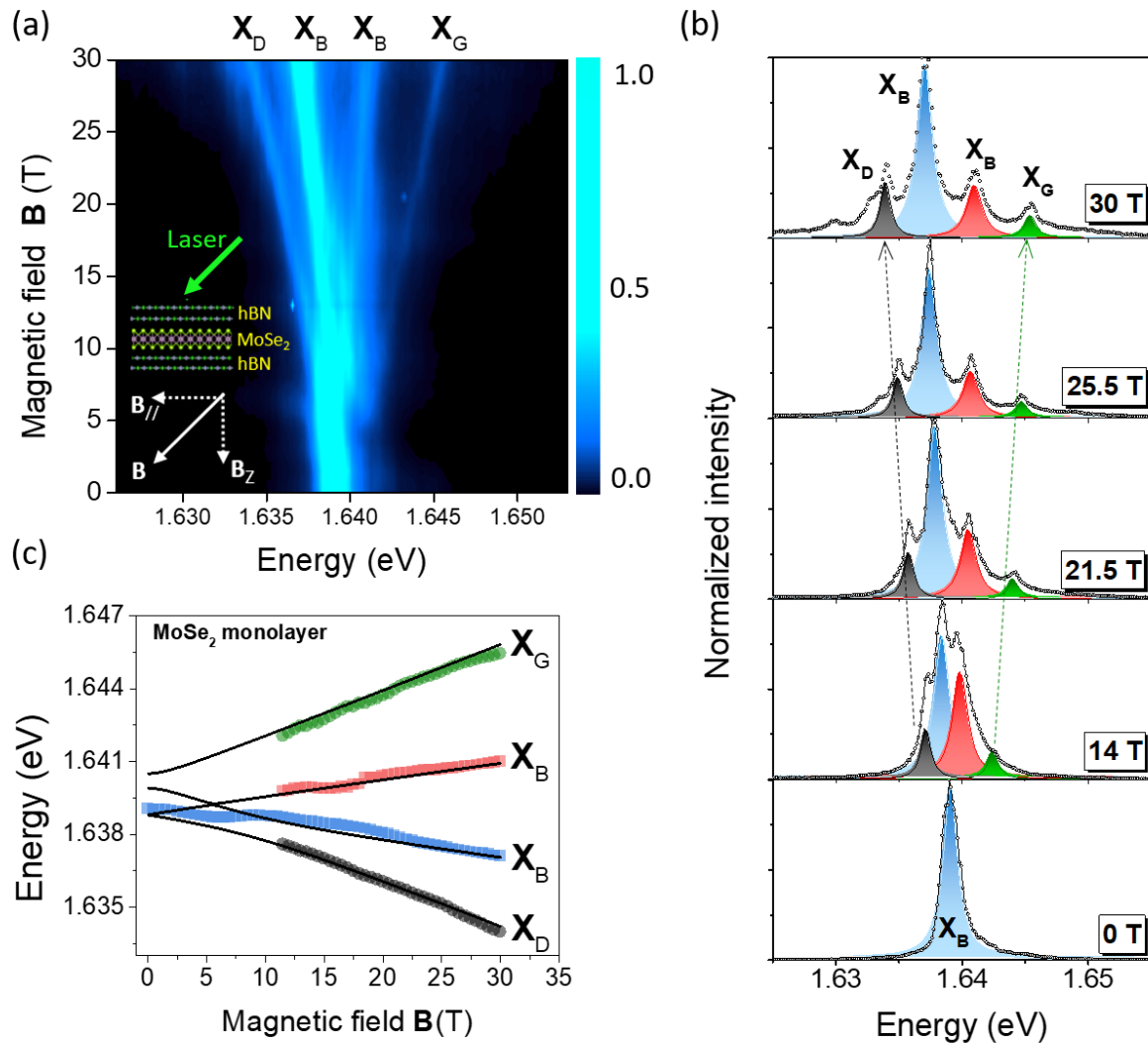


Figure 3 – Tilted (45°) magnetic field – The 4 mixed excitons states in MoSe<sub>2</sub> monolayer revealed by magneto-photoluminescence. (a) Color map of the variation of the PL intensity as a function of  $B$ ; (b) PL spectra for magnetic fields from 0 to 30 T showing the emergence of the four mixed states (the intensity is normalized to the main exciton line). (c) Magnetic field dependence of the energy of the 4 mixed exciton states. The full lines are fits to the model described in the text. The notations dark exciton ( $X_D$ ), grey exciton ( $X_G$ ) and bright excitons ( $X_B$ ) correspond to the dominant component weight in the exciton wavefunction at low field (See SI7 for the calculation of the weight of the 4 components at high field).

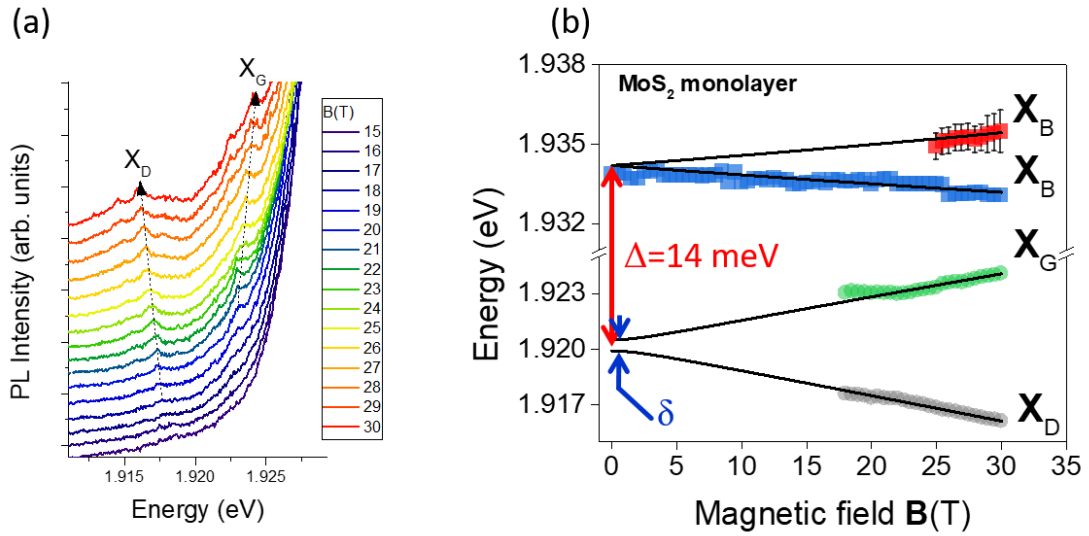


Figure 4 – Tilted (45°) magnetic field – The 4 mixed excitons states in MoS<sub>2</sub> monolayer revealed by magneto-photoluminescence. Magnetic field dependence of the energy of the 4 mixed exciton states. The full lines are fits to the model described in the text. The notations dark exciton (X<sub>D</sub>), grey exciton (X<sub>G</sub>) and bright excitons (X<sub>B</sub>) correspond to the dominant component weight in the exciton wavefunction at low field (See SI7 for the calculation of the weight of the 4 components at high field).

## References :

- 
- <sup>1</sup> G. Wang, A. Chernikov, M. Glazov, T. Heinz, X. Marie, T. Amand, B. Urbaszek, Review of Modern Physics **90**, 21001 (2018)
  - <sup>2</sup> A. Jones, H. Yu, N. J. Ghimire, S. Wu, G. Aivazian, J.S. Ross, B. Zhao, J. Yan, D. G. Mandrus, D. Xiao, W. Yao, X. Xu, Nature Nano. **8**, 634 (2013)
  - <sup>3</sup> H. Dery, Y. Song, Phys. Rev. B **92**, 125431 (2015)
  - <sup>4</sup> P. Back, S. Zeytinoglu, A. Ijaz, M. Kroner, A. Imamoglu, Phys. Rev. Lett. **120**, 37401 (2018)
  - <sup>5</sup> M. Koperski, M. R. Molas, A. Arora, K. Nogajewski, A. O. Slobodeniuk, C. Faugeras, M. Potemski Nanophotonics **6**, 1289 (2017)
  - <sup>6</sup> G. Wang, C. Robert, A. Suslu, B. Chen, S. Yang, S. Alamdari, I. Gerber, T. Amand, X. Marie, S. Tongay, B. Urbaszek, Nat. Commun. **6**, 10110 (2015).
  - <sup>7</sup> X-X. Zhang, Y. Yumeng, S. Zhao, F. Yang, T. Heinz, Phys. Rev. Lett. **115**, 257403 (2015)
  - <sup>8</sup> F. Withers O. Del Pozo-Zamudio, S. Schwarz, S. Dufferwiel, P.M. Walker, T. Godde, A. Rooney, A. Gholinia, C.R. Woods, P. Blake, S.J. Haigh, K. Watanabe, T. Taniguchi, I.L. Aleiner, A.K. Geim, V.I. Fal'ko, A.I. Tartakovskii, K.S. Novoselov, Nano Lett. **15**, 8223 (2015).
  - <sup>9</sup> A. Arora, M. Koperski, K. Nogajewski, J. Marcus, C. Faugeras, M. Potemski, Nanoscale **7**, 10421 (2015).
  - <sup>10</sup> A. Vinattieri, J. Shah, T. C. Damen, D. S. Kim, L. N. Pfeiffer, M. Z. Maialle, L. J. Sham et al, Phys. Rev. B **50**, 10868 (1993)
  - <sup>11</sup> M. Yang, M. Yang, C. Robert, Z. Lu, D. Van Tuan, D. Smirnov, X. Marie, H. Dery et al, Arxiv 1909.03134 (2019)
  - <sup>12</sup> G. Wang, C. Robert, M. M. Glazov, F. Cadiz, E. Courtade, T. Amand, D. Lagarde, T. Taniguchi, K. Watanabe, B. Urbaszek and X. Marie, PRL **119**, 047401 (2017)
  - <sup>13</sup> M.R. Molas, C. Faugeras, A.O. Slobodeniuk, K. Nogajewski, M. Bartos, D.M. Basko, M. Potemski, 2D Mater. **4**, 021003 (2017)
  - <sup>14</sup> X. Zhang, T. Cao, Z. Lu, Y. Lin, F. Zhang, Y. Wang, Z. Li, J. C. Hone, J. A. Robinson, D. Smirnov, S. G. Louie & T.F. Heinz, Nature Nano **12**, 883 (2017)
  - <sup>15</sup> Y. Zhou, G. Scuri, D. S. Wild, A. A. High, A. Dibos, L. A. Jauregui, C. Shu, K. De Greve, K. Pistunova, A. Y. Joe, T. Taniguchi, K. Watanabe, P. Kim, M. D. Lukin & H. Park, Nature Nano **12**, 856 (2017) |
  - <sup>16</sup> E. Malic, M. Selig, M. Feierabend, S. Brem, D. Christiansen, F. Wendler, A. Knorr, G. Berghäuser, Phys. Rev. Mat **2**, 014002 (2018)
  - <sup>17</sup> T. Deilmann, K. Thygesen Phys. Rev. B **96**, 201113(R) (2017)
  - <sup>18</sup> D.Y. Qiu, T. Cao, S.G. Louie, Phys. Rev. Lett **115**, 176801 (2015) )
  - <sup>19</sup> J. P. Echeverry, B. Urbaszek, T. Amand, X. Marie, I.C. Gerber, Phys. Rev. B **93**, 121107(R) (2016)
  - <sup>20</sup> Z. Lu, D. Rhodes, Z. Li, D.V. Tuan, Z. Jiang, Z. Lian, S.F. Shi, J. Hone, H. Dery, D. Smirnov, 2D Mater. **7**, 015017 (2020)
  - <sup>21</sup> C. Robert, T. Amand, F. Cadiz, D. Lagarde, E. Courtade, M. Manca, T. Taniguchi, K. Watanabe, B. Urbaszek, X. Marie, Phys. Rev. B **96**, 155423 (2017)
  - <sup>22</sup> A O Slobodeniuk and D M Basko, 2D Materials **3**, 035009 (2016)
  - <sup>23</sup> T. Amand, X. Marie, P. Le Jeune, M. Brousseau, D. Robart, J. Barrau, R. Planel, Phys. Rev. Lett. **78**, 1355 (1997)
  - <sup>24</sup> I. V. Mashkov, C. Gourdon, P. Lavallard, and D. Yu Roditchev, Phys. Rev. B **55**, 13761 (1997)
  - <sup>25</sup> C. Robert, M. A. Semina, F. Cadiz, M. Manca, E. Courtade, T. Taniguchi, K. Watanabe, H. Cai, S. Tongay, B. Lassagne, P. Renucci, T. Amand, X. Marie, M. M. Glazov, and B. Urbaszek, Phys. Rev. Mat **2**, 011001(R) (2018)
  - <sup>26</sup> M. Koperski, M.R. Molas, A. Arora, K. Nogajewski, M. Bartos, J. Wyzula, D. Vaclavkova, P. Kossacki, M. Potemski, 2D Mater. **6** 015001 (2019)

- 
- <sup>27</sup> M.R. Molas, A. O. Slobodeniuk, T. Kazimierczuk, K. Nogajewski, M. Bartos, P. Kapuściński, K. Oreszczuk, K. Watanabe, T. Taniguchi, C. Faugeras, P. Kossacki, D. M. Basko, and M. Potemski, *Phys. Rev. Lett.* **123**, 096803 (2019).
- <sup>28</sup> F. Cadiz F. Cadiz, E. Courtade, C. Robert, G. Wang, Y. Shen, H. Cai, T. Taniguchi, K. Watanabe, H. Carrere, D. Lagarde, M. Manca, T. Amand, P. Renucci, S. Tongay, X. Marie and B. Urbaszek, *Phys. Rev. X* **7**, 021026 (2017)
- <sup>29</sup> A. Kormanyos, G. Burkard, M. Gmitra, J. Fabian, V. Zólyomi, N. Drummond, V. Fal'ko et al, *2D Mater.* **2** 022001 (2015)
- <sup>30</sup> M. Goryca, J. Li, A.V. Stier, T. Taniguchi, K. Watanabe, E. Courtade, S. Shree, C. Robert, B. Urbaszek, X. Marie & S.A. Crooker, *Nature Com.* **10**, 4172 (2019)
- <sup>31</sup> R. Pisoni, A. Kormányos, M. Brooks, Z. Lei, P. Back, M. Eich, H. Overweg, Y. Lee, P. Rickhaus, K. Watanabe, T. Taniguchi, A. Imamoglu, G. Burkard, T. Ihn, K. Ensslin, *Phys. Rev. Lett.* **121**, 247701 (2018)
- <sup>32</sup> J. Roch, G. Froehlicher, N. Leisgang, P. Makk, K. Watanabe, T. Taniguchi, R. Warburton, *Nature Nano.* **14**, 432 (2019)
- <sup>33</sup> Z. Jin, X. Li, J.T. Mullen, K.W. Kim, *Phys. Rev. B* **90**, 045422 (2014)
- <sup>34</sup> M. Amani, D.H. Lien, D. Kiriya, J. Xiao, A. Azcatl, J. Noh, S.R. Madhupathy, R. Addou, S.K. Dubey, K. Cho, R.M. Wallace, S.C. Lee, J.H. He, J.W. Ager, X. Zhang, E. Yablonovitch, A. Javey, *Science* **350**, 1065 (2015)
- <sup>35</sup> G. Wang, E. Palleau, T. Amand, S. Tongay, X. Marie, B. Urbaszek, *APL* **106**, 112101 (2015)
- <sup>36</sup> C. Robert, R. Picard, D. Lagarde, G. Wang, J. P. Echeverry, F. Cadiz, P. Renucci, A. Höfgele, T. Amand, X. Marie, I. C. Gerber, B. Urbaszek, *Phys. Rev. B* **94**, 155425 (2016)
- <sup>37</sup> G. Sallen, L. Bouet, X. Marie, G. Wang, C. R. Zhu, W. P. Han, Y. Lu, P. H. Tan, T. Amand, B. L. Liu, and B. Urbaszek, *Phys. Rev. B* **86**, 081301 (2012)
- <sup>38</sup> T. Cao, G. Wang, W. Han, H. Ye, C. Zhu, J. Shi, Q. Niu, P. Tan, E. Wang, B. Liu & J. Feng, *Nat. Commun.* **3**, 887 (2012)
- <sup>39</sup> K. Mak, K. He, J. Shan, T. Heinz, *Nat. Nano.* **7**, 494 (2012)
- <sup>40</sup> H.H. Fang, B. Han, C. Robert, M. A. Semina, D. Lagarde, E. Courtade, T. Taniguchi, K. Watanabe, T. Amand, B. Urbaszek, M. M. Glazov, and X. Marie, *Phys. Rev. Lett.* **123**, 067401 (2019)
- <sup>41</sup> A.V Stier, N. P. Wilson, K. A. Velizhanin, J. Kono, X. Xu, and S. A. Crooker, *Phys. Rev. Lett* **120**, 057405 (2018)

## SUPPLEMENTARY INFORMATION

### *S11. Samples and experimental set-up*

High-quality MoS<sub>2</sub> and MoSe<sub>2</sub> MLs encapsulated in hexagonal boron nitride (hBN) and transferred onto an SiO<sub>2</sub> (80 nm)/Si substrate have been fabricated. Details on sample fabrication can be found in Ref. <sup>1</sup>. The typical thickness of the top (bottom) hBN layer is ~10 (200) nm and the typical in-plane size of the ML is ~10 × 10 μm<sup>2</sup>. The encapsulation of TMD ML in atomically flat hBN layers reduces significantly the inhomogeneous broadening in the photoluminescence (PL) or reflectivity spectra, with typical values in the range 1–3 meV at low temperature<sup>1</sup>.

Low-temperature magneto-PL experiments are performed in the Voigt configuration (magnetic field parallel to the layer plane) or tilted configuration (field oriented 45° with respect to the ML plane) using an optical-fiber-based insert placed in a resistive solenoid producing magnetic fields up to 30 T. The samples are placed on top of an x-y-z piezo-stage kept in gaseous helium at T = 4.2 K. The light from a cw 515 nm laser is coupled to a mono-mode optical fiber with a core diameter of 5 μm and focused on the sample by an aspheric lens (spot diameter around 2 μm). The PL signal is collected by the same lens, injected into a multi-mode optical fiber of 50 μm core diameter, and analyzed by a 0.5 m long monochromator equipped with a charge-coupled-device (CCD) camera.

### *S12. Additional data in MoS<sub>2</sub>*

The results presented in Fig.1 (brightening of the dark exciton in MoS<sub>2</sub> in Voigt geometry) have been reproduced in several samples and always give a bright-dark exciton splitting of +14 meV.

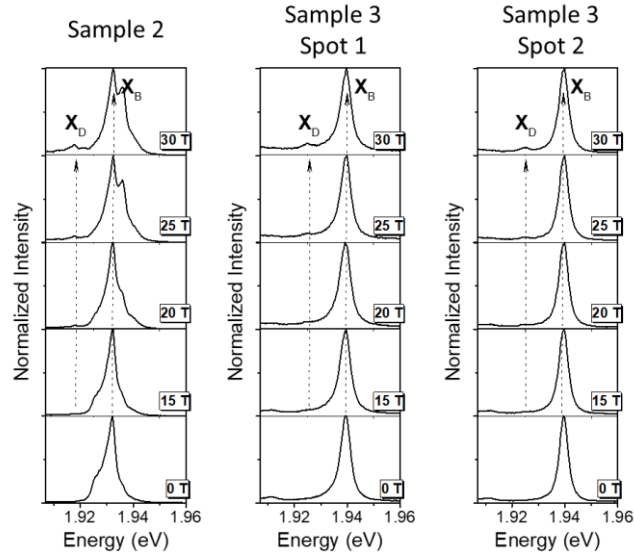


*Figure SI2 : PL spectra for other MoS<sub>2</sub> samples than the one presented in the main text for in plane magnetic fields from 0 to 30 T showing the emergence of the brightened dark exciton X<sub>D</sub> 14 meV below the bright exciton X<sub>B</sub>.*

### SI3. Excitation power dependence of the dark exciton

We checked that the optical transition we interpreted as the dark exciton of MoS<sub>2</sub> has a PL intensity that varies linearly with excitation power. We can thus safely exclude that it originates from a defect state.

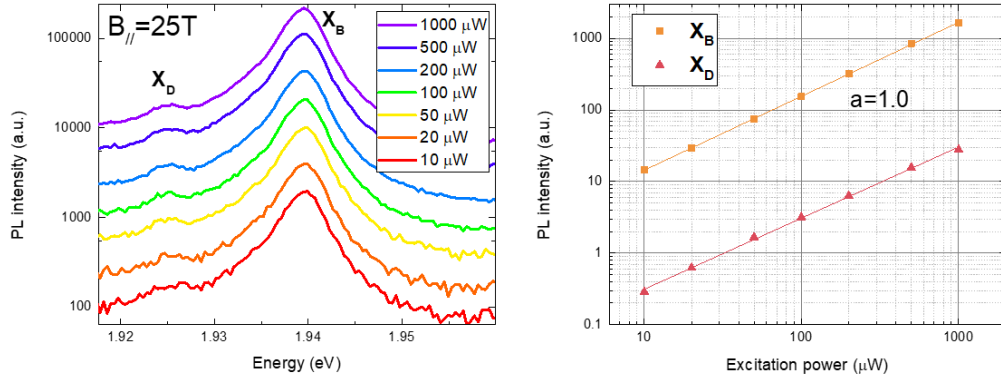


Figure SI3 : (Left) Normalized PL spectra for MoS<sub>2</sub> samples for in plane magnetic field of 25T as a function of excitation power. The spectra are shifted for clarity. (Right) Integrated intensity of bright and dark exciton lines at 25T as a function of power.

### SI4. Additional data in MoSe<sub>2</sub>

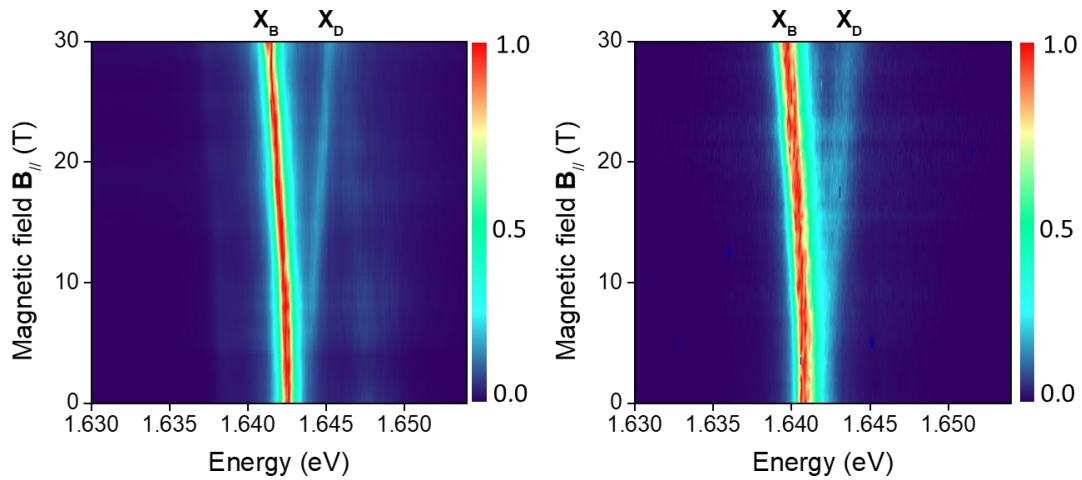


Figure SI4 : PL spectra for MoSe<sub>2</sub> samples for in plane magnetic fields from 0 to 30 T at two different spot positions than the one presented in the main text. The PL intensity of the bright exciton has been normalized at each field.

### SI5. Raw data of MoS<sub>2</sub> in tilted field

In tilted field, the spot size is bigger and consequently the lines are broader. Nevertheless, we can clearly distinguish the two dark states emerging at high field. We present here the raw data as a color plot.

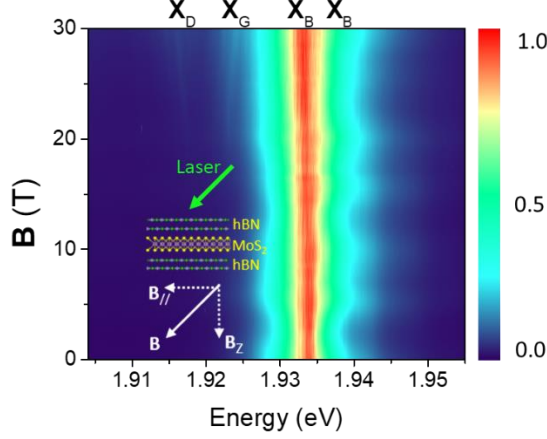


Figure SI5 : PL spectra for MoS<sub>2</sub> in tilted field. The PL intensity of the bright exciton has been normalized at each field.

### SI6. Exciton fine structure in tilted magnetic field

The TMD materials such as WSe<sub>2</sub>, WS<sub>2</sub>, MoS<sub>2</sub>, MoSe<sub>2</sub> and MoTe<sub>2</sub> crystallize in hexagonal structure which is invariant under the symmetry operations of the D<sub>3h</sub> group<sup>2</sup>. In such materials, the conduction bands Bloch amplitudes  $U_m^\gamma$  in non-equivalent  $K_\pm$  valleys belong to the D<sub>3h</sub> representations:  $\{\Gamma_8, \Gamma_9\}$ , the latter being split by spin-orbit interaction, while the topmost valence bands (A) ones belong to  $\Gamma_7$  representation<sup>3</sup>. The electron-hole Bloch-amplitude pair functions built with these states belong thus to the representation product  $\Gamma_9 \otimes \Gamma_7^* \otimes \Gamma_{env}$  and  $\Gamma_8 \otimes \Gamma_7^* \otimes \Gamma_{env}$  in notations of ref.<sup>4</sup>. Restricting ourselves to 1s exciton ground states, we have  $\Gamma_{env} = \Gamma_1$ , so that, all the single particle representations being two-dimensional, we obtain four exciton states in the A series with symmetry  $\Gamma_9 \otimes \Gamma_7^* = \Gamma_5 + \Gamma_6$  and four others with symmetry  $\Gamma_8 \otimes \Gamma_7^* = \Gamma_3 + \Gamma_4 + \Gamma_6$ . However, using coupling tables, it can be seen that only the  $\Gamma_6$ -excitons of  $\Gamma_9 \otimes \Gamma_7^*$  and  $\Gamma_3$ - and  $\Gamma_4$ -excitons of  $\Gamma_8 \otimes \Gamma_7^*$  are direct excitons, the  $\Gamma_6$  doublet and  $\Gamma_4$  singlet excitons being only coupled to light (dipole allowed). Defining the hole Bloch amplitude by  $U_{\mp 1/2}^{h,7} = \pm \hat{K}(U_{\pm 1/2}^7)$ ,  $\hat{K}$  being the time-reversal operator, these excitons Bloch amplitudes are denoted here by :

$$\Psi_{\pm 1}^6 = U_{\mp 1/2}^9 \otimes U_{\mp 1/2}^{h,7}, \quad (S1)$$

coupled to  $\sigma^\pm$  photons respectively, and

$$\Psi^4 = \frac{i}{\sqrt{2}} (U_{+1/2}^8 \otimes U_{-1/2}^{h,7} + U_{-1/2}^8 \otimes U_{+1/2}^{h,7}) \quad (S2)$$

$$\Psi^3 = \frac{1}{\sqrt{2}} (U_{+1/2}^8 \otimes U_{-1/2}^{h,7} - U_{-1/2}^8 \otimes U_{+1/2}^{h,7})$$

$\Psi^4$  being the only one coupled to  $\pi^z$  photons (the Z-exciton mode<sup>1</sup>).

**i. Coulomb exchange and spin-orbit interaction.**

Beside direct Coulomb interaction, these excitons experience electron-hole exchange, so that, in the direct exciton manifold with basis  $\mathbf{B} = \{\Psi_{+1}^6, \Psi_{-1}^6, \Psi^3, \Psi^4\}$  the effective exciton Hamiltonian, taking into account exchange and spin-orbit interaction<sup>5</sup>, can be written as<sup>1</sup>:

$$H_{exch} = \frac{1}{2} \begin{pmatrix} \Delta & 0 & 0 & 0 \\ 0 & \Delta & 0 & 0 \\ 0 & 0 & -\Delta - \delta & 0 \\ 0 & 0 & 0 & -\Delta + \delta \end{pmatrix} \quad (S3)$$

We turn now to the action of an external magnetic field  $\mathbf{B}$  applied to the sample in any direction, and derive the corresponding Zeeman effective Hamiltonian.

We write its components in spherical coordinates as:

$$\mathbf{B} = (B \sin \theta \cos \varphi, \quad B \sin \theta \sin \varphi, \quad B \cos \theta)^T .$$

**ii. Longitudinal part of the magnetic field:  $B_z \mathbf{e}_z = B \cos \theta \mathbf{e}_z$**

This component belongs to  $\Gamma_2$  representation of  $D_{3h}$ . Thus, a pure longitudinal magnetic field splits the states  $\Psi_{+1}^6, \Psi_{-1}^6$ , and couples the states  $\Psi^3$  and  $\Psi^4$ . Using the coupling tables of ref. <sup>4</sup>, we have shown that this Hamiltonian can be presented in the form<sup>2</sup>:

$$H_{Bz} = \frac{1}{2} \mu_B B \cos(\theta) \begin{pmatrix} g_z^B & 0 & 0 & 0 \\ 0 & -g_z^B & 0 & 0 \\ 0 & 0 & 0 & i g_z^D \\ 0 & 0 & -i g_z^D & 0 \end{pmatrix} \quad (S4)$$

**iii. Transverse part of the magnetic field:  $\mathbf{B}_{//} = B \sin \theta \cos \varphi \mathbf{e}_x + B \sin \theta \sin \varphi \mathbf{e}_y$**

We have  $B_x \pm i B_y = B \sin \theta e^{\pm i \varphi}$  which transforms like the spin operators  $\hat{S}_x \pm i \hat{S}_y$ . These components and operators belong to  $\Gamma_5$  two-dimensional representation of  $D_{3h}$ . The product of exciton states representations:

$\Gamma_6^* \otimes \Gamma_6 = \Gamma_6 \otimes \Gamma_6 = \Gamma_1 + \Gamma_2 + \Gamma_6$ ,  $\Gamma_3^* \otimes \Gamma_3 = \Gamma_3 \otimes \Gamma_3 = \Gamma_1 = \Gamma_4^* \otimes \Gamma_4$ ,  $\Gamma_3^* \otimes \Gamma_4 = \Gamma_3 \otimes \Gamma_4 = \Gamma_2$ , do not contain  $\Gamma_5$  representation, but  $\Gamma_6^* \otimes (\Gamma_3 + \Gamma_4) = 2\Gamma_5$ . So it can be deduced that the transverse field only couples the  $\Psi^3$  and  $\Psi_{\pm 1}^6$  excitons one hand, and the  $\Psi^4$  and  $\Psi_{\pm 1}^6$  excitons, with *a priori* two different coupling constants. The Zeeman Hamiltonian contribution of the transverse field can thus be presented under the form:

$$H_{B//} = \frac{1}{2\sqrt{2}} \mu_B B \sin(\theta) \begin{pmatrix} 0 & 0 & g_{//} e^{-i\varphi} & i g_{//} e^{-i\varphi} \\ 0 & 0 & -g_{//} e^{+i\varphi} & i g_{//} e^{+i\varphi} \\ g_{//} e^{+i\varphi} & -g_{//} e^{-i\varphi} & 0 & 0 \\ -i g_{//} e^{+i\varphi} & -i g_{//} e^{-i\varphi} & 0 & 0 \end{pmatrix} \quad (S5)$$



, where we have assumed for simplicity that the two coupling constants are opposite. This can be justified by the fact that only the conduction electrons contribute significantly to the coupling.

The total Hamiltonian is thus, in the general case:

$$\boxed{H^X = H_{exch}^X + H_{B_z}^X + H_{B_{//}}^X} \quad (S6)$$

We have checked that this Hamiltonian is strictly equivalent to the one written in ref.<sup>6</sup> expressed in a different basis fabricated with states in each valley. Indeed, the secular equation of the Eigen-equation of the system is independent of the basis choice and is given by:

$$\begin{aligned} & [(\Delta - 2\lambda)^2 - (g_z^b \mu_B B \sin\theta)^2][(\Delta + 2\lambda)^2 - (g_z^d \mu_B B \cos\theta)^2 - \delta^2] + \\ & + 2(g_{//} \mu_B B \sin\theta)^2 (\Delta^2 - 4\lambda^2 + g_z^b g_z^d \cos^2\theta) + (g_{//} \mu_B B \cos\theta)^4 = 0 \end{aligned}$$

As expected, it is clearly seen that the four Eigen-energies  $\lambda$  do not depend on the azimuthal angle  $\varphi$  of the magnetic field.

Note that this equation is also invariant when changing  $g_{//}$  by  $-g_{//}$ , and by changing both signs of  $g_z^b$  and  $g_z^d$ , which shows that the sign of these two g-factors are linked. In the Hamiltonian (S4) the bright g factor  $g_z^b$  is defined with the usual convention  $g_z^b \mu_B B_z = E_{\psi_{+1}^6} - E_{\psi_{-1}^6}$  so that with  $g_z^b < 0$  the energy of the bright exciton with the electron in K+ ( $|\Psi_{+1}^6\rangle$  state) decreases when  $B_z$  increases. The definition of the dark g factor  $g_z^d$  is not so obvious in the Hamiltonian (S4). To explain our convention we can write the two dark states in each valley:

$$\begin{aligned} |K_+^d\rangle &= U_{+1/2}^8 \otimes U_{-1/2}^{h,7} = \frac{|\Psi^3\rangle - i|\Psi^4\rangle}{\sqrt{2}} \\ |K_-^d\rangle &= U_{-1/2}^8 \otimes U_{+1/2}^{h,7} = -\frac{|\Psi^3\rangle + i|\Psi^4\rangle}{\sqrt{2}} \end{aligned}$$

In the Hamiltonian (S4),  $g_z^d$  is defined so that with  $g_z^d < 0$  the energy of the dark exciton with the electron in K+ ( $|K_+^d\rangle$  state) decreases when  $B_z$  increases.

Thanks to the fitting of Fig. 3c, we experimentally confirmed that both  $g_z^b$  and  $g_z^d$  are indeed negative in MoSe<sub>2</sub> with our conventions.

**SI7. Calculation of the weight of each component in the mixed exciton states in tilted field at 30 T**

The solid lines in Fig.3c and Fig.4 are obtained by numerically calculate the eigenvalues of Hamiltonian (S6). By calculating the eigenvectors we can determine the weight of each component ( $\Psi_{+1}^6, \Psi_{-1}^6, \Psi^3, \Psi^4$ ) in the exciton states at 30 T. The results presented in the tables below for MoSe<sub>2</sub> and MoS<sub>2</sub> show that the states are strongly mixed.

Calculated eigenvalues	1.6342 eV	1.6371 eV	1.6409 eV	1.6458 eV
$\Psi_{+1}^6$	0.2479	0.7521	0	0
$\Psi_{-1}^6$	0	0	0.9325	0.0675
$\Psi^3$	0.3964	0.1331	0.0302	0.4402
$\Psi^4$	0.3557	0.1148	0.0373	0.4923

Table S1: Weight in module of the 4 components ( $\Psi_{+1}^6, \Psi_{-1}^6, \Psi^3, \Psi^4$ ) in the 4 eigenvalues of MoSe<sub>2</sub> calculated at 30 T for  $\theta=45^\circ$ . The main component is shown in grey.

Calculated eigenvalues	1.9161 eV	1.9241 eV	1.9332 eV	1.9354 eV
$\Psi_{+1}^6$	0.0052	0	0.9948	0
$\Psi_{-1}^6$	0	0.0118	0	0.9882
$\Psi^3$	0.5346	0.4572	0.0024	0.0057
$\Psi^4$	0.4602	0.5310	0.0028	0.0061

Table S2: Weight in module of the 4 components ( $\Psi_{+1}^6, \Psi_{-1}^6, \Psi^3, \Psi^4$ ) in the 4 eigenvalues of MoS<sub>2</sub> calculated at 30 T for  $\theta=45^\circ$ . The main component is shown in grey.

<sup>1</sup> F. Cadiz *et al*, Phys. Rev. X **7**, 021026 (2017)

<sup>2</sup> C. Robert *et al.*, Phys. Rev. B **96**, 155423 (2017)

<sup>3</sup> A. Kormanyos *et al*, 2D Mater. **2**, 022001 (2015)

<sup>4</sup> G. F. Koster, R. G.Wheeler, J. O. Dimmock, and H. Statz, Properties of the Thirty-Two Point Groups (MIT Press, Cambridge, Massachusetts, 1963).

<sup>5</sup> J. P. Etcheverry *et al*. Phys. Rev. B **93**, 121107(R) (2016)

<sup>6</sup> M.R. Molas *et al*, Phys. Rev. Lett. **123**, 096803 (2019)